Supporting Information

Gradient-band-gap strategy for efficient solid-state PbS quantum-dot sensitized solar cells

Chengfeng Ma, Chengwu Shi *, Kai Lv, Chao Ying, Shasha Fan, Yang Yang
School of Chemistry and Chemical Engineering, Anhui Province Key Laboratory of Advanced Catalytic Materials and Reaction Engineering, Hefei University of Technology, Hefei, 230009, P. R. China

1. Experimental section

1.1 Preparation of rutile TiO_2 nanorod arrays

Preparation of 60 nm thick TiO_2 compact layers [1]: 60 nm thick TiO_2 compact layers were prepared by a hydrolysis-pyrolysis process using a mildly acidic solution of titanium isopropoxide in isopropanol (0.23 M titanium isopropoxide and 0.013 M HCl). The above mildly acidic solution was dropped on FTO, spin-coated at 2000 rpm for 60 s, and then heated at 500 ˚C for 30 min. The 60 nm thick TiO_2 compact layers were deposited on FTO.

Preparation of rutile TiO_2 nanorod arrays [2, 3]: The rutile TiO_2 nanorod array was grown on 60 nm thick TiO_2 compact layers by hydrothermal method. Briefly, the hydrothermal method was carried out in a stainless-steel autoclave with a Teflon liner of 50 mL capacity. Then, 520 μL of titanium isopropoxide was added into 40 mL of 6 M hydrochloric acid and sonicated for 25 min to obtain the 44 mM titanium isopropoxide aqueous grown solution. Subsequently, two pieces of FTO with 60 nm thick TiO_2 compact layers were positioned tilted inside the Teflon liner with the active layer facing the wall. The 40 mL aqueous grown solution was transferred into the Teflon liner and kept at 170 ˚C for 96 min. After the autoclave was naturally cooled to room temperature in air, the two pieces of FTO were taken out from the autoclave, rinsed thoroughly, and annealed at 450 ˚C for 30 min in air prior to use.

* Corresponding author. Tel.: +86 551 62901450; fax: +86 551 62901450.
E-mail address: shicw506@foxmail.com, shicw506@hfut.edu.cn

The surface and cross-sectional SEM images, XRD pattern, and UV-Vis absorption spectrum of the resulting TiO_2 nanorod array were shown in Figure S1. The TiO_2 nanorod array possessed a length of 570 nm, diameter of 20 nm, and an areal density of 560 μm^{-2}. The weak diffraction peaks at 2θ=36.1° and 62.8° appeared correspond to the spacing of the (101) and (002) planes of the tetragonal rutile phase (JCPDS: 71-0650), and a preferred orientation along the (101) plane was observed. The absorption onset of the TiO_2 nanorod array was 413 nm and the corresponding band bap was 3.0 eV.

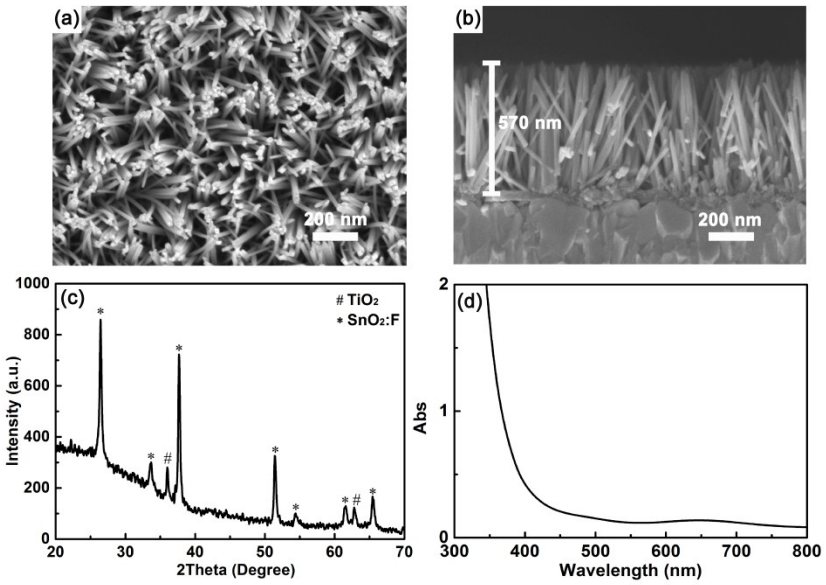

Figure S1 Surface (a) and cross-sectional (b) SEM images, XRD pattern (c), and UV-Vis absorption spectrum (d) of the TiO_2 nanorod array.

1.2 The architecture and fabrication of all solid-state PbS quantum-dot sensitized solar cells

The 60 nm thick TiO_2 compact layers, rutile TiO_2 nanorod arrays, and the PbS quantum-dots (QDs) were successively deposited on FTO. The preparation of the PbS QDs was in an open ambient atmosphere and the room temperature was 26 ˚C. Subsequently, 40 μL of *spiro*-OMeTAD solution in chlorobenzene was dropped and spin-coated at 4000 rpm for 30 s. Finally, a 60-nm-thick gold electrode was deposited on the *spiro*-OMeTAD layer. The active areas of 0.09 cm^{-2} were defined by the black

and opaque film with the square aperture (3 mm × 3 mm) adhered on FTO. Figure S2 showed the architecture of the solid-state PbS quantum-dot sensitized solar cells (QDSCs).

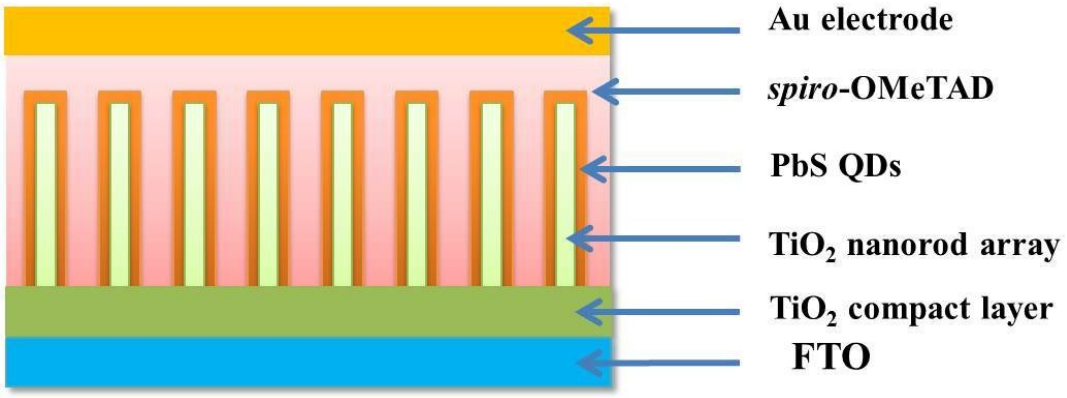

Figure S2 The architecture of all solid-state PbS QDSCs.

1.3 Characterizations

The ultraviolet photoelectron spectroscopy (UPS) was performed on an ESCALAB 250Xi electron spectrometer with a monochromatic Al Kα source (300 W) under a pressure of approximately 2×10^{-10} Pa using an He I (21.22 eV) gas discharge lamp. The photoluminescence (PL) spectra was obtained by exciting the PbS QD sensitized TiO_2 nanorod arrays at 850 nm with a standard 450 W xenon CW lamp. The transmission electron microscope (TEM, JEOL-2010) was observed at an acceleration voltage of 200 kV and the high-resolution transmission electron microscope (HRTEM, FEI Tecnai G2 F30) was carried out at an acceleration voltage of 300 kV. The measurement of X-ray photoelectron spectroscopy (XPS), scanning electron microscopy (SEM), X-ray diffraction (XRD), ultraviolet-visible spectroscopy (UV-Vis), the incident photon-to-electron conversion efficiency (IPCE) spectra, electrochemical impedance spectroscopy (EIS) and photovoltaic performance were the same as in our previous reports [3,4].

2. The deposition of PbS QDs can be successfully simplified from three-step spin-coating to two-step spin-coating

2.1 The preparation of PbS QDs using three-step spin-coating and two-step spin-

coating

Three-step spin-coating (shown in Figure S3): The preparation of PbS QDs using three-step spin-coating was the same as in our previous report [4]. Briefly, 100 μL of 5 mM $Pb(NO_3)_2$ solution in methanol/water (95/5, v/v), 100 μL of 2 mM Na_2S solution in methanol/water (95/5, v/v), and 100 μL of 1 % EDT solution in ethanol were successively dropped and spin-coated at 1500 rpm for 20 s. The three-step spin-coating cycle was repeated 25 times.

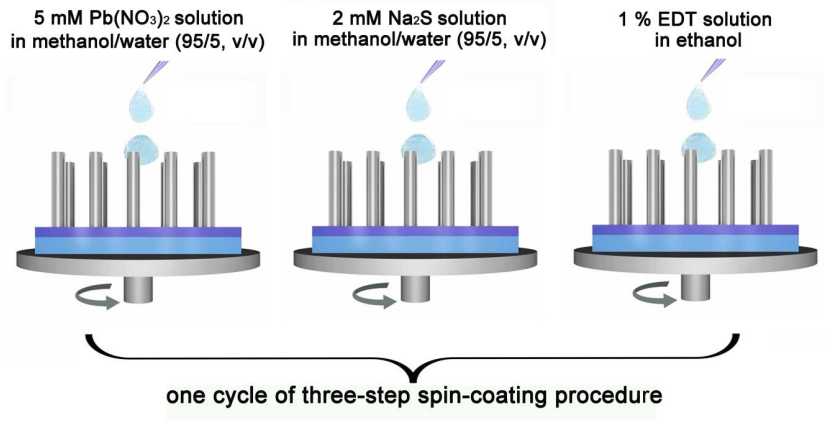

Figure S3 One cycle of three-step spin-coating procedure.

Two-step spin-coating (shown in Figure S4): The mixed solution of 2 mM Na_2S and 1.5 mM EDT in methanol/water (95/5, v/v) was prepared. Subsequently, 100 μL of 5 mM $Pb(NO_3)_2$ solution in methanol/water (95/5, v/v) and 100 μL of 2 mM Na_2S and 1.5 mM EDT mixed solution in methanol/water (95/5, v/v) were respectively dropped and spin-coated at 1500 rpm for 20 s. The two-step spin-coating cycle was repeated 25 times.

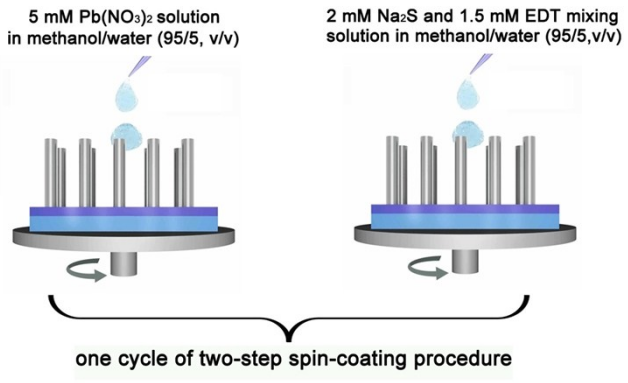

Figure S4 One cycle of two-step spin-coating procedures.

2.2 The influence of three-step spin-coating and two-step spin-coating on the PbS QDs

Figure S5 showed the surface SEM images, XRD patterns and UV-Vis absorption spectra of PbS QDs using three-step spin-coating and two-step spin-coating procedures. From the surface SEM images, the compact and full-covering PbS QDs were successfully deposited on the top and inside the TiO_2 nanorod arrays and there was no obvious difference of the surface morphology using three-step spin-coating or two-step spin-coating procedures. From the XRD patterns and UV-Vis absorption spectra, both PbS QDs showed diffraction peaks at 2θ=30.4° corresponding to the spacing of the (200) plane of the cubic PbS (JCPDS:78-1057). The absorption onsets of PbS QDs were almost the same in the range of 680–720 nm.

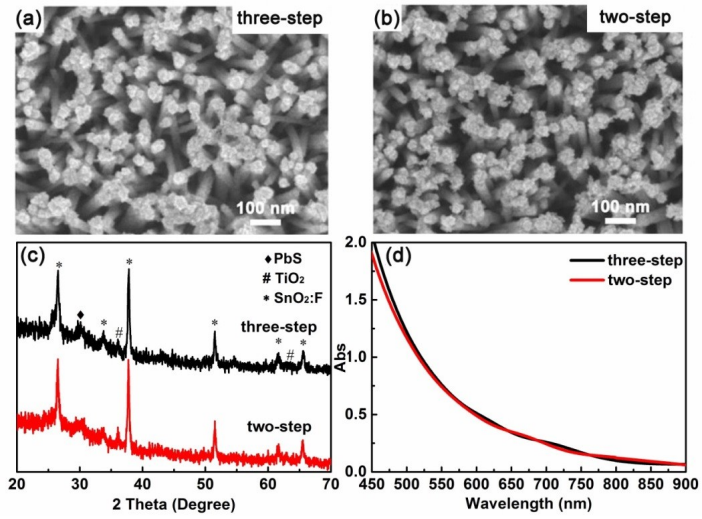

Figure S5 Surface SEM images, XRD patterns and UV-Vis absorption spectra of PbS QDs using three-step spin-coating and two-step spin-coating procedures.

Figure S6 showed the XPS spectra of PbS QDs using three-step spin-coating and two-step spin-coating procedures. To the Pb-EDT complex, the Pb $4f_{7/2}$ and $4f_{5/2}$ peaks were located at 137.96 eV and 142.83 eV with a peak splitting of 4.87 eV, and the S $2p_{3/2}$ and S $2p_{1/2}$ peaks were located at 161.67 eV and 162.94 eV with a peak splitting of 1.27 eV. For PbS, the Pb $4f_{7/2}$ and Pb $4f_{5/2}$ peaks of PbS were located at 137.40 eV and 142.27 eV with a peak splitting of 4.87 eV, and the S $2p_{3/2}$ and S $2p_{1/2}$ peaks were located at 160.60 eV and 161.80 eV with a peak splitting of 1.20 eV [5]. Therefore, the Pb 4f and S 2p peaks in PbS QDs can be divided into two parts of the Pb-EDT complex and PbS, and the corresponding integral area ratios were listed in Table S1. It can be seen that the content of the Pb-EDT complex using the three-step spin-coating procedure was slightly lower than that using the two-step spin-coating procedure in PbS QDs. The content of the Pb-EDT complex and PbS in the PbS QDs can be adjusted by changing the Na_2S and EDT concentration of the mixing solution in two-step spin-coating procedure. Because the Pb-EDT/PbS ratio of 0.44-0.46:1 in the PbS QDs using the two-step spin-coating procedure was less than the EDT/Na_2S concentration ratio of 1.5:2 in the mixing solution, the chemical reaction of Pb^{2+} and S^{2-} in Na_2S was relative easier than that of Pb^{2+} and S in EDT.

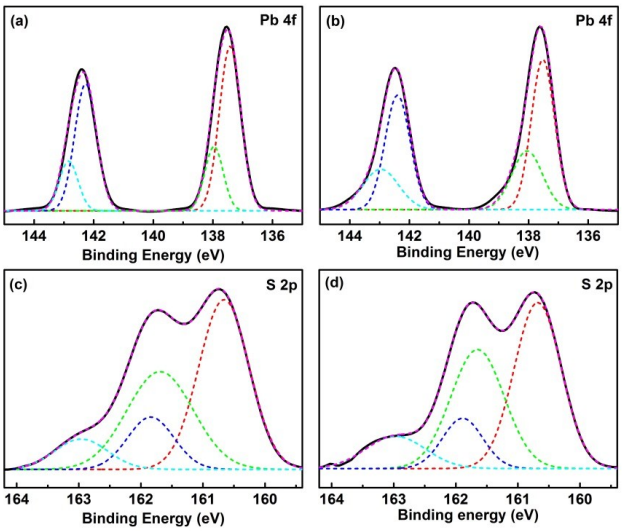

Figure S6 XPS spectra of PbS QDs using three-step spin-coating (a,c) and two-step spin-coating (b,d) procedures.

Table S1 The integral area ratios of Pb-EDT complex and PbS in PbS QDs

Pb-EDT/PbS	Pb $4f_{7/2}$	Pb $4f_{5/2}$	S $2p_{3/2}$	S $2p_{1/2}$
Three-step spin-coating	0.33:1.00	0.33:1.00	0.69:1.00	0.67:1.00
Two-step spin-coating	0.44:1.00	0.46:1.00	0.81:1.00	0.78:1.00

2.3 The photovoltaic performance of PbS QDSCs using three-step spin-coating and two-step spin-coating

Figure S7 showed the photocurrent-photovoltage characteristics of PbS QDSCs using three-step and two-step spin-coating procedures. The QDSCs using the three-step spin-coating procedure exhibited a PCE of 3.79 %, along with a open-circuit voltage (V_{oc}) of 0.54 V, a short-circuit photocurrent density (J_{sc}) of 11.90 mA·cm^{-2}, and a fill factor (FF) of 0.59. The QDSCs using the two-step spin-coating procedure exhibited a PCE of 3.81 %, along with a V_{oc} of 0.55 V, a J_{sc} 11.35 mA·cm^{-2}, and an FF of 0.61. These photovoltaic performance parameters of QDSCs were almost the same whether using the three-step spin-coating or two-step spin-coating procedures. Combined with the results of SEM, XRD, UV-Vis and XPS, it was concluded that the preparation of PbS QDs can be successfully simplified from three-step spin-coating procedure to two-step spin-coating procedure using the SILAR method. This simplification was the key to constructing gradient-band-gap PbS QDs by only changing the EDT concentration in the Na_2S and EDT mixed solution of the two-step spin-coating procedure.

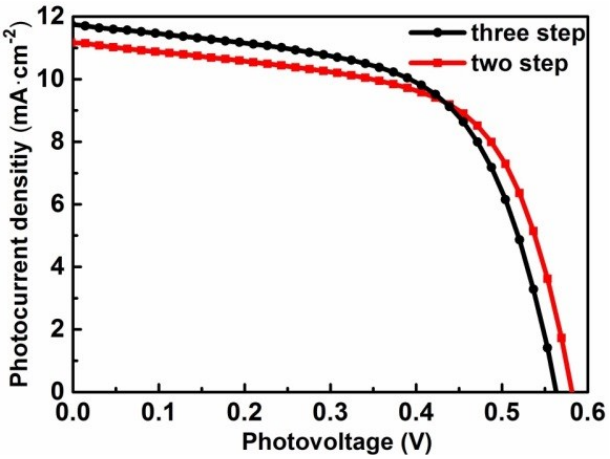

Figure S7 Photocurrent-photovoltage characteristics of PbS QDSCs using three-step and two-step spin-coating procedures.

3. The XRD pattern, UV-Vis absorption spectra, XPS spectra, surface SEM images, TEM images and HRTEM images of PbS QDs using the mixed solution of 2 mM Na_2S and 1.5 mM/3 mM/6 mM EDT by two-step spin-coating

Figure S8 showed the XRD patterns of the PbS QDs with the different spin-coating cycles of 20 times and 8 times using the mixed solution of 2 mM Na_2S and 1.5 mM EDT. When the spin-coating cycles decreased from 20 times to 8 times, the diffraction peaks of the PbS QDs divided from one peak to two peaks. The result may be due to the inhomogeneous and diverse distribution of EDT in the PbS QDs from every spin-coating cycle and different spin-coating cycle times. For the spin-coating cycle of 8 times, the average crystal size of the PbS QDs was difficult to be calculated because the diffraction peaks of the PbS QDs divided from one peak to two peaks.

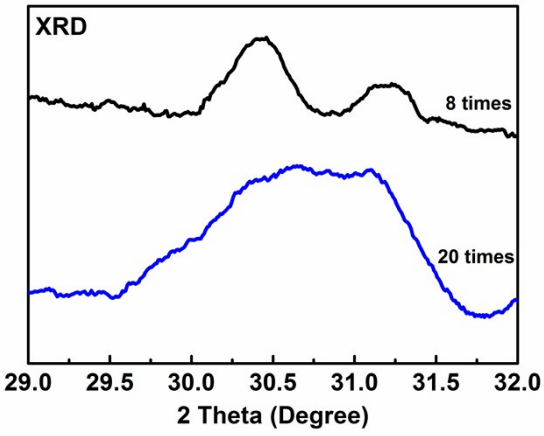

Figure S8 XRD patterns of the PbS QDs with the different spin-coating cycles of 20 times and 8

times using the mixed solution of 2 mM Na_2S and 1.5 mM EDT.

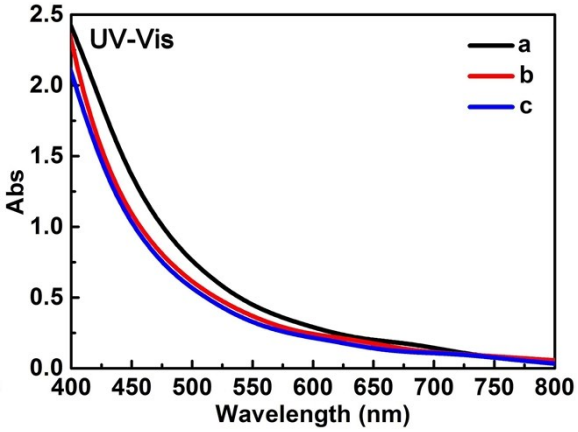

Figure S9 UV-Vis absorption spectra of PbS QDs using the mixed solution of 2 mM Na_2S and 1.5 mM (a) 3 mM (b) 6 mM (c) EDT.

Figure S9 showed the UV-Vis spectra of PbS QDs using the mixed solution of 2 mM Na_2S and 1.5 mM/3 mM/6 mM EDT. It was found that the absorption onsets of the PbS QDs blue-shifted from 716 nm to 700 nm and 681 nm with the increase of the EDT concentration in the mixed solution from 1.5 mM to 3 mM and 6 mM.

Figure S10 showed the Pb 4f and S 2p XPS spectra of PbS QDs using the mixed solution of 2 mM Na_2S and 1.5 mM/3 mM/6 mM EDT, and the corresponding integral area ratios of the Pb-EDT complex and PbS were listed in Table S2 [5]. With the increase of the EDT concentration, the content of the Pb-EDT complex in the PbS QDs increased. These results revealed that the chemical composition of PbS QDs can be easily adjusted by only changing the EDT concentration in the mixed solution of 2 mM Na_2S and 1.5 mM/3 mM/6 mM EDT.

Table S2 The integral area ratios of the Pb-EDT complex and PbS in PbS QDs using the mixed solution of 2 mM Na_2S and 1.5 mM/3 mM/6 mM EDT.

Pb-EDT/PbS	Pb $4f_{7/2}$	Pb $4f_{5/2}$	S $2p_{3/2}$	S $2p_{1/2}$
1.5 mM	0.39:1.00	0.42:1.00	0.79:1.00	0.83:1.00
3 mM	0.79:1.00	0.78:1.00	1.31:1.00	1.20:1.00
6 mM	1.25:1.00	1.21:1.00	2.19:1.00	2.08:1.00

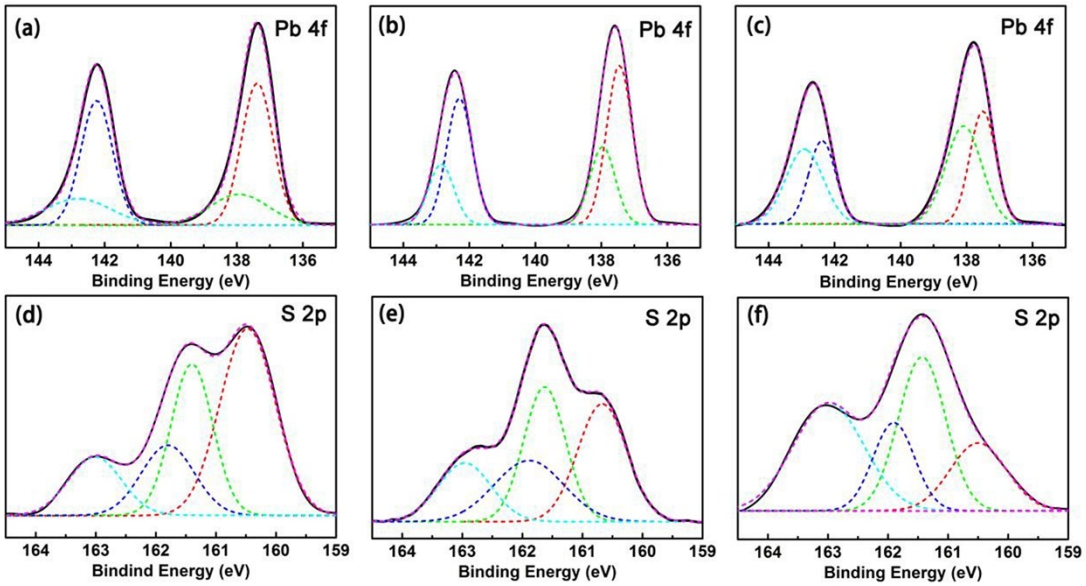

Figure S10 Pb 4f and S 2p XPS spectra of PbS QDs using the mixed solution of 2 mM Na_2S and 1.5 mM (a, d), 3 mM (b, e), and 6 mM (c, f) EDT.

Figure S11 showed the surface SEM images, TEM images and HRTEM images of PbS QDs using the mixed solution of 2 mM Na_2S and 1.5 mM/3 mM/6 mM EDT. It can be seen that the three PbS QDs were full-covering on the surface of the TiO_2 nanorod. The full-covering PbS QDs can prevent direct contact between the TiO_2 nanorod arrays and the *spiro*-OMeTAD and further suppress the charge recombination. The lattice spacing of 0.25 nm should be assigned to the crystal (101) phase of the rutile TiO_2 (JCPDS:71-0650) and the lattice spacing of 0.29 nm should be assigned to the crystal (200) phase of the cubic PbS (JCPDS:78-1057). The results were in accordance with the XRD result shown in Figure S5. From Figure S11 (d-f), it was found that the PbS QD layer thickness for the spin-coating cycles of 8 times using the mixing solution of 2 mM Na_2S and 1.5 mM EDT was about 6 nm. Also, the PbS QD layer thickness using the mixing solution of 2 mM Na_2S and 3/6 mM EDT was about 4-5 nm.

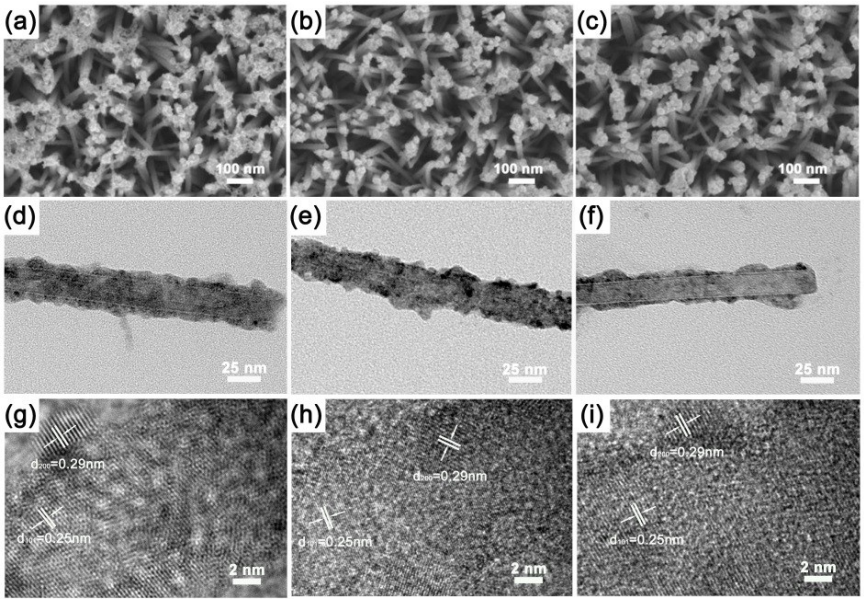

Figure S11 Surface SEM images, TEM images, HR-TEM images of PbS QDs using the mixed solution of 2 mM Na_2S and 1.5 mM (a, d, e), 3 mM (b, e, h), and 6 mM (c, f, i) EDT.

4. Analysis of UPS spectra

Figure S12 showed the UPS spectra of PbS QDs using the mixed solution of 2 mM Na_2S and 1.5 mM/3 mM/6 mM EDT. From UPS with a He(I) discharge lamp of 21.22 eV, the Fermi energy level (E_F) and valence band maximum (E_V) of PbS QDs can be determined by the intersections of the linear portion of high and low binding energy region with the baseline. For the EDT concentration of 1.5 mM, 3 mM, and 6 mM, the intersection values of the high binding energy region (E_H) were 16.39 eV, 16.44 eV, and 16.50 eV, respectively, and the Fermi energy levels ($E_F = E_H$ - 21.22 eV) were -4.83 eV, -4.78 eV, and -4.72 eV, respectively. The intersection values of the low binding energy region (E_L) were 0.60 eV, 0.58 eV, and 0.54 eV, and the valence band maximums ($E_V = E_F - E_L$) were -5.43 eV, -5.36 eV, and -5.26 eV, respectively. According to the band gap values (1.73 eV, 1.77 eV, and 1.82 eV) of PbS QDs, the corresponding conduction band minimums ($E_C = E_V + E_g$) were -3.70 eV, -3.59 eV, and -3.44 eV.

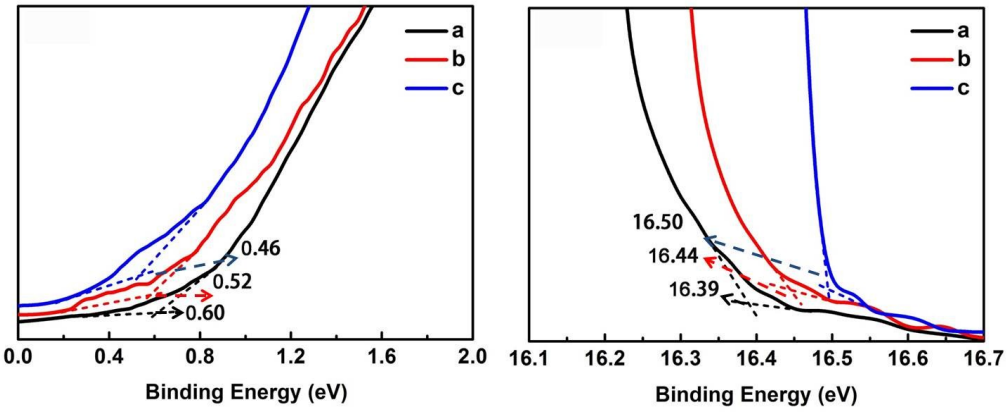

Figure S12 UPS spectra of PbS QDs using mixed solutions of 2 mM Na_2S and 1.5 mM (a), 3 mM (b), and 6 mM (c) EDT.

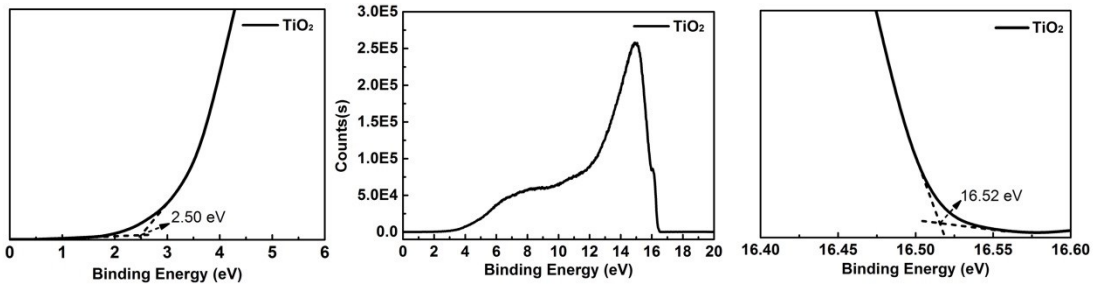

Figure S13 UPS spectra of TiO_2 nanorod array

Figure S13 showed the UPS spectra of the TiO_2 nanorod array. The intersection values of the high binding energy region (E_H) and the low binding energy region (E_L) were 16.52 eV and 2.50 eV, respectively. The band gap value of the TiO_2 nanorod array was 3.0 eV. Similarly, the Fermi energy level, valence band maximum and conduction band minimum were -4.70 eV, -7.20 eV, and -4.20 eV, respectively. The valence band maximum of *spiro*-OMeTAD was -5.20 eV from the literature [6].

5. The optimization of all solid-state gradient-band-gap PbS QDSCs

The modification of the TiO_2 nanorod array: 100 μL of 1 % 3-mercaptopropionic acid (3-MPA) solution in ethanol was dropped on the TiO_2 nanorod array. After waiting for 30 s, the spin-coater was started and spin-coated at 1500 rpm for 20 s. The 3-MPA modified TiO_2 nanorod array was obtained.

The optimization of the cycle times with spin-coating the mixing solution of 2 mM Na_2S and 1.5 mM EDT solution: Figure S14 showed the schematic diagram of

the gradient-band-gap PbS QDs with different cycle times of 10, 12, 14, 16. The spin-coating parameter of the *spiro*-OMeTAD layer was 4000 rpm for 30 s, and the room temperature in the SILAR preparation of PbS QDs was 26 ˚C. Figure S15 showed the photocurrent-photovoltage characteristics and Table S3 listed the photovoltaic performance parameters of the corresponding solid-state QDSCs.

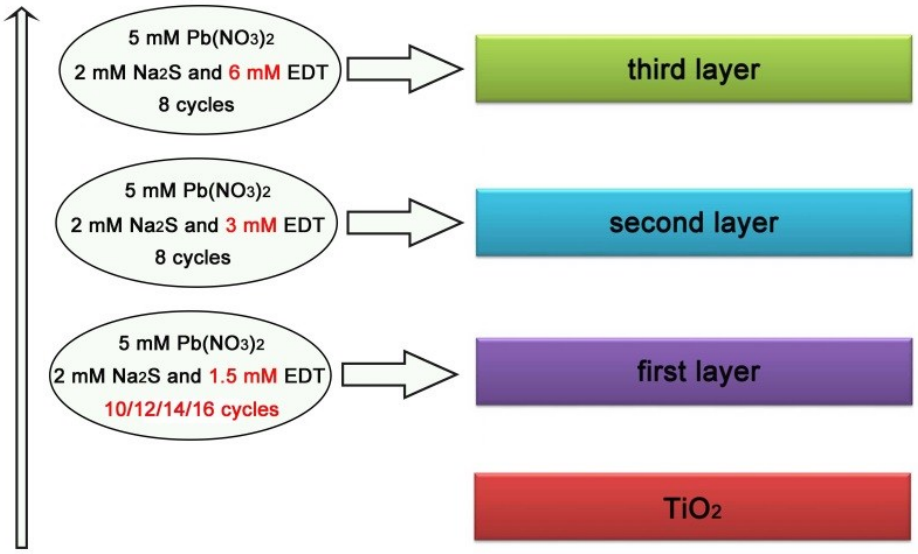

Figure S14 Schematic diagram of gradient-band-gap PbS QDs with different cycle times of 10, 12, 14, and 16.

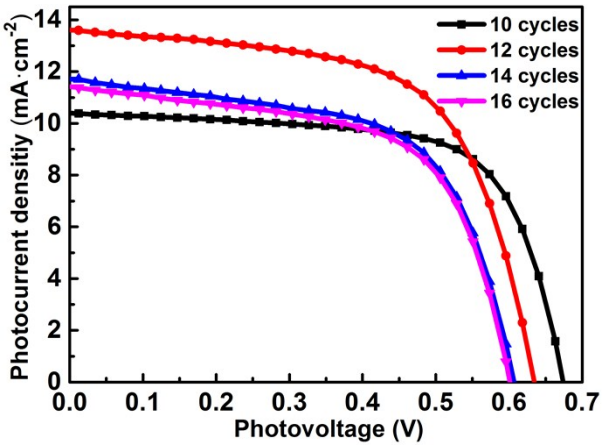

Figure S15 Photocurrent-photovoltage characteristics of the corresponding solid-state QDSCs with different cycle times of 10, 12, 14, and 16.

Table S3. Photovoltaic performance parameters of the corresponding solid-state QDSCs with different cycle times of 10, 12, 14, and 16.

Solar cells	V_{oc} (V)	J_{sc} (mA·cm^{-2})	FF	PCE (%)
10 cycles	0.68	10.41	0.67	4.74
12 cycles	0.63	13.62	0.62	5.37
14 cycles	0.61	11.72	0.61	4.32
16 cycles	0.60	11.19	0.61	4.19

The optimization of *spiro*-OMeTAD layer and the reduction of the room temperature in the SILAR preparation of PbS QDs: When the spin-coating parameters of the *spiro*-OMeTAD layer were changed from 4000 rpm for 30 s to 3000 rpm for 60 s, the room temperature in the SILAR preparation of PbS QDs was reduced from 26 ˚C to 19 ˚C and the cycle times of spin-coating the mixed solution of 2 mM Na_2S and 1.5 mM EDT solution was 12 times, the solid-state gradient-band-gap PbS QDSCs achieved the PCE of 6.29 %, along with a V_{oc} of 0.65 V, a J_{sc} of 15.09 mA·cm^{-2}, and an FF of 0.64 under 1 sun, and the corresponding IPCE spectra was shown in Figure S16. When the irradiation intensity was reduced from 1 sun to 0.5 sun, the PCE increased from 6.29 % to 7.21 %, along with a V_{oc} of 0.60 V, a J_{sc} of 8.92 mA·cm^{-2}, and an FF of 0.67.

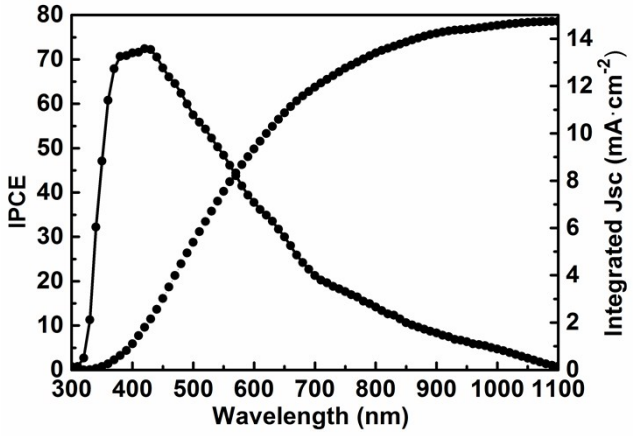

Figure S16 IPCE spectrum of the best gradient-band-gap PbS QDSC.

6. The influence of different PbS QD layers on the photovoltaic performance of the corresponding QDSCs

Table S4 Photovoltaic performance parameters of QDSCs with different PbS QD layers.

PbS QD layer (spin-coating cycle times)	V_{oc} (V)	J_{sc} (mA·cm^{-2})	FF	PCE (%)
First layer (12)	0.54	5.71	0.40	1.23
	0.55	5.84	0.42	1.35
	0.55	6.10	0.48	1.60
	0.56	7.49	0.44	1.84
First layer(12) +Second layer(8)	0.62	8.45	0.57	3.00
	0.58	10.66	0.55	3.43
	0.58	10.56	0.58	3.56
	0.58	11.27	0.58	3.77
First layer(12) +Second layer(8) +Third layer(8)	0.66	14.26	0.62	5.87
	0.65	15.82	0.58	5.91
	0.64	15.33	0.62	6.11
	0.65	15.52	0.63	6.28

On 2019-02-19, the QDSCs with different PbS QD layers (A. First layer of 12 spin-coating cycles, B. First layer of 12 spin-coating cycles + Second layer of 8 spin-coating cycles, C. First layer of 12 spin-coating cycles + Second layer of 8 spin-coating cycles + Third layer of 8 spin-coating cycles) have been fabricated and the corresponding photovoltaic performance parameters was shown in Table S4. Because the PCE of QDSCs with the three-step gradient-band-gap was the highest, the result implied that the gradient-band-gap was best constructed using multiple gradients. In this work, only the spin-coating cycles of First layer were optimized (shown in Table S3). The optimizations of the spin-coating cycles for Second layer, for Third layer, and for combination with First layer, Second layer and Third layer should be worthy of further study.

7. The storage stability of the PbS QDSCs

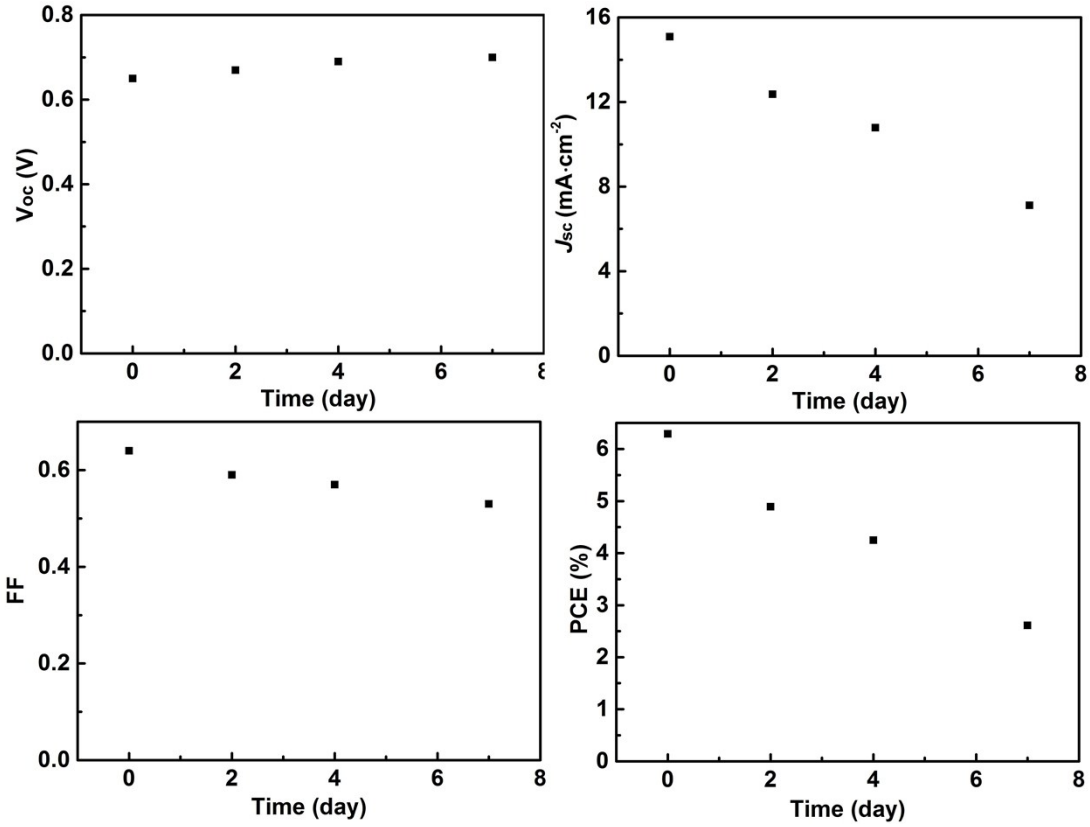

Figure S17 The evolution of photovoltaic performance parameters of the best PbS QDSCs.

When the QDSC with the PCE of 6.29 % was stored in open ambient atmosphere of our laboratory, the evolution of photovoltaic performance parameters with the storage time was shown in Figure S17. The V_{oc} slightly increased, the FF slightly decreased and the J_{sc} obviously decreased with the increase of the storage time. The PCE decreased from 6.29 % to 2.61 % of 7 days. The result demonstrated that the introduction of EDT can improve the PbS QD ambient stability, which was consistent with the literature reports (Seok et al., the reference [10] in the main text). Comparing the PCE of 6.29 % and the PCE of Table S4, it can be found that the fabricating experiment of the gradient-band-gap PbS QDSCs can be reproduced. Certainly, the decrease of PCE with the increase of storage times should be because the defect of the incomplete coordinating lead and the dangling sulfur bond in PbS QDs using SILAR was much than that using the hot injection method.

References

[1] J. Zhang, C. Shi, J. Chen, Y. Wang, M. Li, *J. Solid State Chem.* **2016**, 238, 223.

[2] Xiao, G. Shi, C. Zhang, Z. Li, N. Li, L. *J. Solid State Chem.* **2017**, 249, 169.

[3] G. Xiao, C. Shi, L. Li, Z. Zhang, C. Ma, K. Lv, *Ceram. Int.* **2017**, 43, 12534.

[4] Z. Zhang, C. Shi, L. Kai, C. Ma, G. Xiao, L. Ni, *J. Energy. Chem.* **2018**, 27, 1214.

[5] C. Ma, C. Shi, K. Lv, Z. Shao, W. Chen, *J. Mater. Sci.-Mater. E.* **2018**, 29, 11783-11789.

[6] M. Zhang, D. Zhao, L. Chen, N. Pan, Huang, C. Cao, H. M. Chen, *Dyes Pigments* **2017**, 146, 589.